EFFECT OF REYNOLDS NUMBER ON SEPARATION BUBBLES ON CONTROLLED-DIFFUSION COMPRESSOR BLADES IN CASCADE

Garth V. Hobson[*]
Denis J. Hansen[**], **David G. Schnorenberg**[**] **and Darren V. Grove**[**]
Department of Aeronautics and Astronautics
Turbopropulsion Laboratory
Naval Postgraduate School
Monterey, California

ABSTRACT

A detailed experimental investigation of second-generation, controlled-diffusion, compressor stator blades at an off-design inlet-flow angle was performed in a low-speed cascade wind tunnel primarily using laser-Doppler velocimetry (LDV). The object of the study was to characterize the off-design flowfield and to obtain LDV measurements of the suction surface boundary layer separation which occurred near mid chord. The effect of Reynolds number on the flow separation in the regime of 210,000 to 640,000 was investigated. Surface flow visualization showed that at the low Re. no. the mid-chord separation bubble started laminar and reattached turbulent within 20% chord on the suction side of the blade. The extent of the bubble compared very well with the measured blade surface pressure distribution which showed a classical plateau and then diffusion in the turbulent region. LDV measurements of the flow reversal in the bubble were performed. At the intermediate Re. no. the boundary layer was transitional before the bubble which had decreased significantly in size (down to 10% chord). At the highest Re. no. the flow was turbulent from close to the leading edge, and three-dimensional flow reversal as a result of endwall effects appeared at approximately 80% chord which did not reattach.

NOMENCLATURE

C	chord length [mm]
Cp	coefficient of pressure, $\left(p - p_\infty\right) / \frac{1}{2}\rho W_{ref}^2$
d	normal distance from the blade [mm]
H	shape factor
p	pressure
S	blade pitch, or spacing [mm]
x	axial direction (also the vertical direction in the cascade) [mm]
u'	axial velocity turbulent fluctuation
U	axial velocity
v'	tangential velocity turbulent fluctuation
V	tangential velocity
W	total velocity, $\sqrt{U^2 + V^2}$
y	tangential direction (also the horizontal direction) [mm]
β	flow angle (measured from the axial) [degrees]
δ	displacement thickness
θ	momentum thickness
η	normal to the chordwise direction [mm]
ρ	density
ξ	chordwise direction [mm]

[*] Associate Professor
[**] Graduate Student

Report Documentation Page

Form Approved
OMB No. 0704-0188

1. REPORT DATE	2. REPORT TYPE	3. DATES COVERED
FEB 2001	**N/A**	**-**

4. TITLE AND SUBTITLE	5a. CONTRACT NUMBER
Effect of Reynolds Number on Separation Bubbles on Controlled-Diffusion Compressor Blades in Cascade	5b. GRANT NUMBER
	5c. PROGRAM ELEMENT NUMBER
6. AUTHOR(S)	5d. PROJECT NUMBER
Garth V. /Hobson; Denis J. /Hansen; David G. /Schnorenberg; Darren V. /Grove	5e. TASK NUMBER
	5f. WORK UNIT NUMBER
7. PERFORMING ORGANIZATION NAME(S) AND ADDRESS(ES) **Naval Post Graduate School 1 University Circle Monterey, CA 93943**	8. PERFORMING ORGANIZATION REPORT NUMBER
9. SPONSORING/MONITORING AGENCY NAME(S) AND ADDRESS(ES)	10. SPONSOR/MONITOR'S ACRONYM(S)
	11. SPONSOR/MONITOR'S REPORT NUMBER(S)

12. DISTRIBUTION/AVAILABILITY STATEMENT
Approved for public release, distribution unlimited

13. SUPPLEMENTARY NOTES

14. ABSTRACT

15. SUBJECT TERMS

16. SECURITY CLASSIFICATION OF:			17. LIMITATION OF ABSTRACT	18. NUMBER OF PAGES	19a. NAME OF RESPONSIBLE PERSON
a. REPORT	b. ABSTRACT	c. THIS PAGE			
unclassified	**unclassified**	**unclassified**	**UU**	**12**	

Standard Form 298 (Rev. 8-98)
Prescribed by ANSI Std Z39-18

ω mass-averaged total pressure loss coefficient

subscripts

ref upstream reference conditions
0 stagnation conditions
1 upstream, or lower, traverse slot
2 downstream, or upper, traverse slot

INTRODUCTION

"At high flight altitudes and low flight speeds, the Reynolds number of the flow through the inlet stages of a compressor becomes so low that their performance is often impaired." (Johnsen and Bullock, 1965) The present study used a set of second-generation controlled-diffusion (CD) stator blades in cascade to study the effect of Reynolds number which would be experienced with such flight condition changes. The blades were designed as stator 67B and tested as stage 67B by Gelder et. al. (1989). The design-point Reynolds number, based on chord, for stator 67B was almost one million at sea level, and this was estimated to decrease to 200,000 at 15,000 m. Three Reynolds numbers (namely 640,000, 380,000 and 210,000) were tested with ten stator 67B blades in cascade in the Naval Postgraduate School, Low-Speed Cascade Wind Tunnel.
Many earlier cascade wind tunnel tests have been conducted to study the effect of Reynolds number on blade element performance, most notably those by Rhoden (1956), Horlock et. al. (1964), Schlichting and Das (1970), Evans (1971) and Roberts (1975). The last three works were also concerned with the effects of free-stream turbulence, which is also important to blade performance. All these two-dimensional cascade tests indicated a deterioration in performance when the Reynolds number was decreased below 100,000, however; most of the earlier tests were conducted at Reynolds numbers well below 500,000 (Johnsen and Bullock, 1965).

Thus the present study has three motivating points. First the Reynolds number range which the cascade (and blade chord of 12.7 cm) could produce is more representative of flight conditions. Second the blade profiles were the mid section of a modern design which had been rig tested (Gelder, et. al., 1989). Third the present study is seen as a challenging test case for turbulence and transition models used in numerical prediction of separated flows.

Sanger (1982) designed stator 67A with controlled-diffusion blade profiles to replace the original double-circular-arc profiles of Stage 67. The object of the study was to implement a design optimization procedure in replacing the original blades with the same blade count. These blade profiles were extensively tested in the NPS cascade wind tunnel (Elazar, 1988, Hobson and Shreeve, 1993). The subsequent design and testing of stator 67B by Gelder et. al. (1989) was to improve on the performance of the stator 67A blade row by halving the blade count whilst still performing the same amount of flow turning. The blades of stator 67B were more highly loaded than those of stator 67A and thus are more cambered, however the leading edge shapes of 67B were made elliptic (as opposed to the circular leading edge of 67A) in an attempt to eliminate leading-edge separation which was prevalent on stator 67A.

EXPERIMENTAL APPARATUS AND PROCEDURE

The Low-Speed Cascade Wind Tunnel of the NPS Turbopropulsion Laboratory was used throughout this study. The inlet flow uniformity and periodicity had been thoroughly documented by Elazar (1988), with 20 Stator 67A blades in the cascade. A schematic of the cascade is shown in Fig. 1. Ten Stator 67B profiles were installed in the test section.

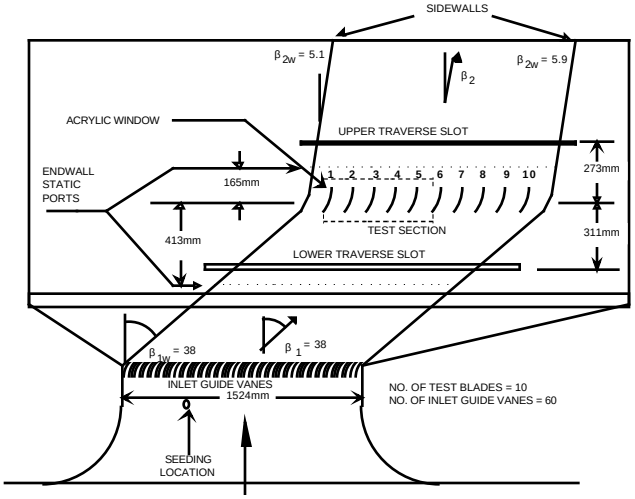

Fig. 1 Low-speed cascade wind tunnel schematic.

Each blade had an aspect ratio of 1.996 and the solidity of the blade row was 0.835. Fig. 2 shows the blade profile and the machine coordinates are tabulated in the Appendix. Table 1 contains a summary listing of the geometrical parameters of the cascade test section. A two-component laser-Doppler velocimeter was used for the LDV measurements at the station locations denoted in Fig 3. The velocity components measured were the vertical (U), or axial velocity and the horizontal (V), or tangential velocity and all the measurements were taken in coincidence mode. One micron size oil mist particles were used as the seed material. These were introduced into the flow at the location shown on Fig. 1.

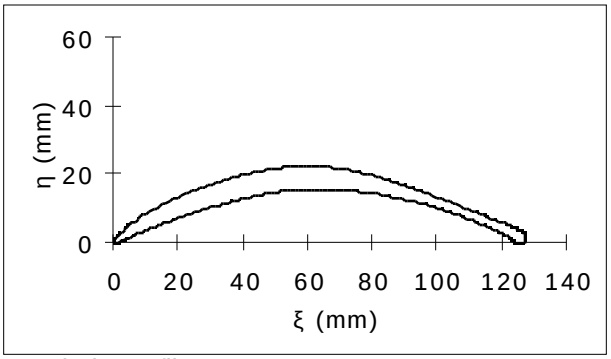

Fig. 2 Blade profile.

Table 1. Test section specifications.

Blade Type	Stator 67B Controlled Diffusion
Number of Blades	10
Blade Spacing	152.40 mm
Chord	127.14 mm
Setting Angle	16.3° +/- 0.1°
Span	254.0 mm

All measurements recorded were for 1000 data points and no editing was used to present the data. Suitable tilting and yawing of the LDV was performed to allow access as close to the blade surfaces as possible, particularly during the boundary layer surveys as shown on Fig 3. During the low Reynolds number (210,000)

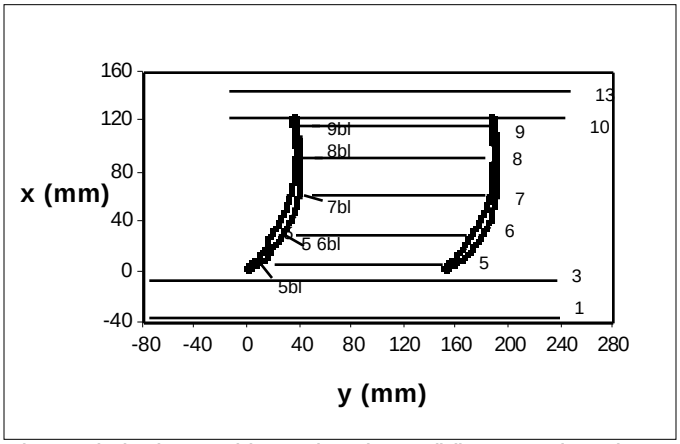

Fig. 3 Pitchwise and boundary layer (bl) survey locations with station designations.

Loss measurements were performed with a traversing five-hole probe at the upper traverse slot (Fig 1) for the “near design” inlet flow angle test case. Flow unsteadiness due to trailing edge separation precluded these measurements at the increased incidence. Blade surface pressure measurements were recorded from an instrumented blade which had 48 pressure ports machined into its surface. Surface flow visualization was performed with a titanium dioxide and kerosene mixture. Both video of the developing surface flow patterns and still photography of the end result once the mixture had dried on the blade surfaces were recorded.

Table 2 Estimated measurement uncertainty

ITEM	DESCRIPTION	UNCERTAINTY
X, Y	Distance from blade surface	0.025mm
P_t	Plenum pressure	25 Pa
p	Pressure (Scanivalve)	12 Pa
P_{atm}	Atmospheric pressure	35 Pa
T_t	Plenum temperature	0.2°C
	LDV clock counter	1 n-sec
κ	Beam half angle	0.3°
L	Focal length	7.6 mm
λ	Wavelength	0.1%
d_f	Fringe spacing	0.3%
U, V	Particle velocity	0.33% @ 10 m/s 0.65% @ 100 m/s

The estimated measurement uncertainties are given in Table 2. The uncertainties in parameters κ, L and λ were given by the manufacturer. The fringe spacing was calculated as $d_f = \lambda / \sin \kappa$. Since particles do not follow the flow exactly, the uncertainty in the velocity can be larger than the uncertainty in the particle velocity.

RESULTS AND DISCUSSION

Blade Surface Pressure Distributions

Measurements were performed on the cascade at the high Reynolds number of 640,000 by Hansen (1995) at the "near design" inlet flow angle of 36 degrees. Fig. 4 shows the results of the blade surface pressure

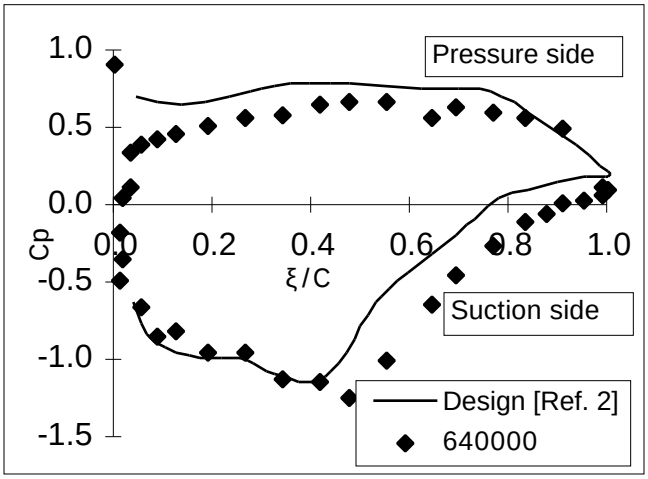

Fig. 4 Blade surface pressure distribution at 36° inlet flow angle.

distribution measurements in terms of the coefficient of pressure, Cp, plotted along the blade chord at various positions given by the ratio ξ/C. Gelder's design intent for stator 67B (Gelder et. al., 1989) is shown plotted with the solid black line. Five-hole probe surveys upstream and downstream of the blade row yielded an axial velocity density ratio ($AVDR = \overline{\rho_2 U_2} / \overline{\rho_1 U_1}$, where the overbar represents mass averaged quantities) of 1.03 and the loss coefficient, $\omega = \left(\bar{p}_{02} - \bar{p}_{01}\right) / \left(\bar{p}_{01} - \bar{p}_1\right)$, was 0.030. The experimentally determined loss coefficient, of the stator blade element at 50% span, in stage 67B by Gelder et. al. (1989) was reported to be 0.029.

The Cp distribution at the three Reynolds numbers are shown in Fig. 5. All these measurements were performed at an inlet flow angle (β) of 38 degrees (Schnorenberg, 1996). The distribution on the suction side of the blade for the high Reynolds number rose continuously from the minimum pressure location at 40% chord, and thus showed no indication of flow separation. The distribution at the intermediate Reynolds number of 380,000 implied a separation region between approx. 50% and 65% chord. At the low Reynolds number (210,000) the distribution implied a separation region between 45% and 70% chord because of the plateau in the mid chord region of the suction surface. The separation region had moved forward with

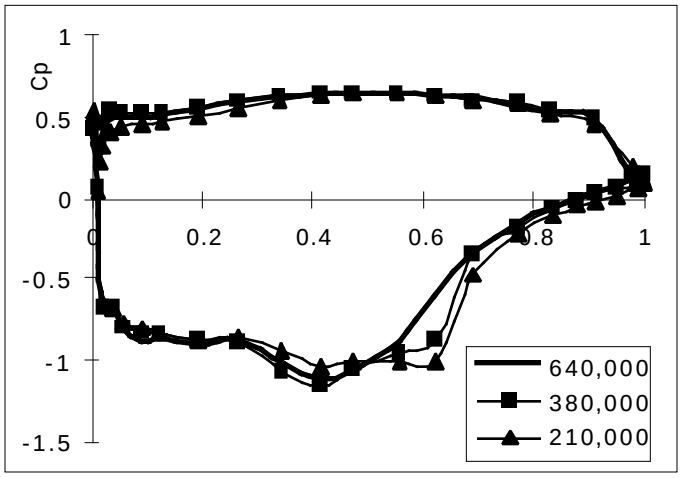

Fig. 5 Blade surface pressure distribution at 38^o inlet flow angle.

decreasing Reynolds number and the separation bubble had also affected the minimum suction peak by reducing its magnitude. Both these observations were consistent with earlier separation bubble studies as reported by Rhoden (1965), Horlock et. al. (1964) and Roberts (1975).

Flow Visualization

Surface flow visualization was performed on blades 3 and 4 in the cascade at the three Reynolds numbers. The flow pattern at the high Reynolds number, shown in Fig. 6, revealed that the flow was three dimensional in the trailing edge region due to the formation of corner vortices in the vicinity of the cascade endwalls.

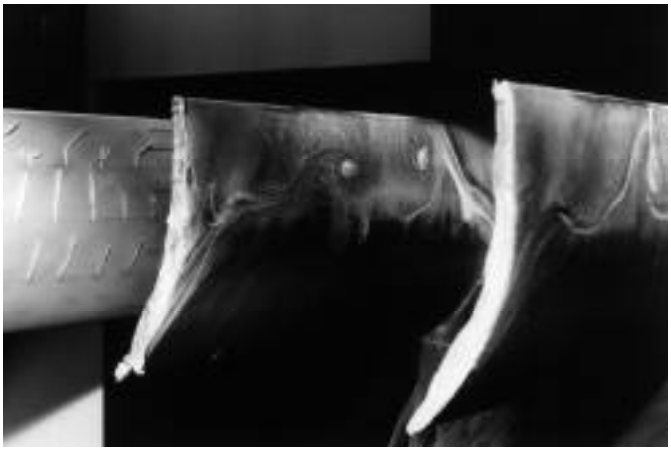

Fig. 6 Surface flow visualization at 640,000 Reynolds number and 38^o inlet flow angle.

In addition the flow was not symmetric about the midspan due to the different boundary layer thicknesses between the two end walls which resulted in different vortex locations on the blade surface.
The flow visualization at the intermediate Reynolds number, shown in Fig. 7, indicated two-dimensional flow along most of the midspan section as well as good periodicity between the blades. A region of transitional (or spanwise intermittent) separation was noted and measured at a position corresponding to 46% chord with a re-attachment point at 57% chord. By transitional separation is meant that where the boundary layer had undergone transition to turbulent flow, either naturally or due to local surface roughness, separation had not yet occurred. This gave rise to the regions where no TiO_2 was present, i.e. the vertical black streaks on the blade at midspan. In the regions along the span of the blade were transition of the boundary layer was suppressed then laminar separation did occur as was noted by the spanwise intermittent separation bubbles. The actual separation point (without the surface fluid) was closer to the trailing edge as gravitational effects had moved the fluid in the separation bubble downward toward the leading edges. The measured separation region correlated well with the Cp distribution which indicated a separation region between approximately 50% and 65% chord.

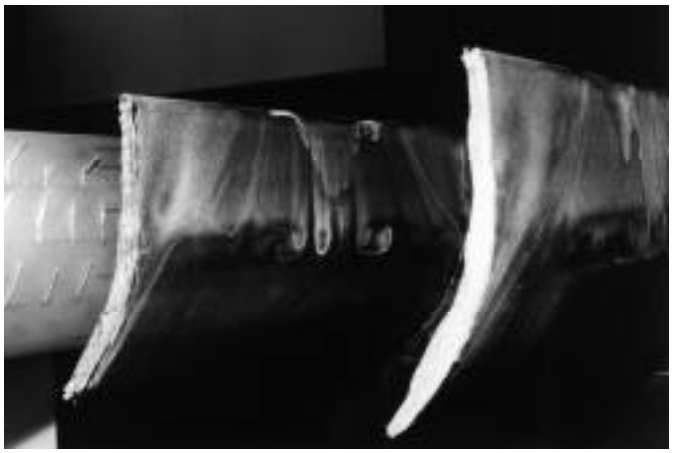

Fig. 7 Surface flow visualization at 380,000 Reynolds number and 38° inlet flow angle.

The flow visualization at the low Reynolds number, shown in Fig. 8, indicated two-dimensional flow along most of the midspan section. A region of laminar separation was noted and measured at a position corresponding to 39% chord with a re-attachment point at approximately 63% chord. A small amount of TiO_2/ kerosene fluid was suspended in this region. Again taking into account the gravitational effects on the suspended fluid, the measured separation region correlated well with the Cp distribution, which indicated a separation region between approximately 45% and 70% chord.

Fig. 8 Surface flow visualization at 210,000 Reynolds number and 38° inlet flow angle.

Inlet and Wake Profiles

Inlet flow field surveys were conducted at station 1, 30% of an axial chord ahead of the blade leading edges, over two blade pitches. The summarized inlet flow conditions are presented in Table 3. The total velocity was uniform to within one percent for all the tests, and since the survey points were equi-spaced then the average values tabulated can also be considered as mass-averaged values.

Table 3. Inlet flow conditions

Re. No.	Ave. Inlet Flow Angle (deg.)	Inlet Flow Angle Stand. Dev.	Ave. Inlet Turb. (%)	Inlet Turb. Stand. Dev.
640,000	37.7	1.21	1.6	0.15
380,000	38.2	1.37	1.6	0.14
210,000	38.3	1.48	1.9	0.27

The average inlet flow angle increased by 0.6 degrees when reducing the Reynolds number from the high to the low value, as did the potential effect of the blades on the incoming flow due to the increased pitchwise flow angle variation (or standard deviation). At the high Reynolds number the inlet turbulence was almost 1.6% which was consistent with earlier measurements on the first set of CD blades (Elazar, 1988, and Hobson and Shreeve, 1993). However for the low Reynolds number flow case the turbulence had increased by almost 20% to about 1.9%. The definition of turbulence being;

$$\text{Turbulence} = \frac{1}{2}\frac{\sqrt{(\bar{u}')^2 + (\bar{v}')^2}}{W_{ref}} \qquad [1]$$

The wake total velocity profiles are shown in Fig. 9 for only the highest and lowest Reynolds number flows. These were measured at station 13 which was 20% of an axial chord downstream of the trailing edges.

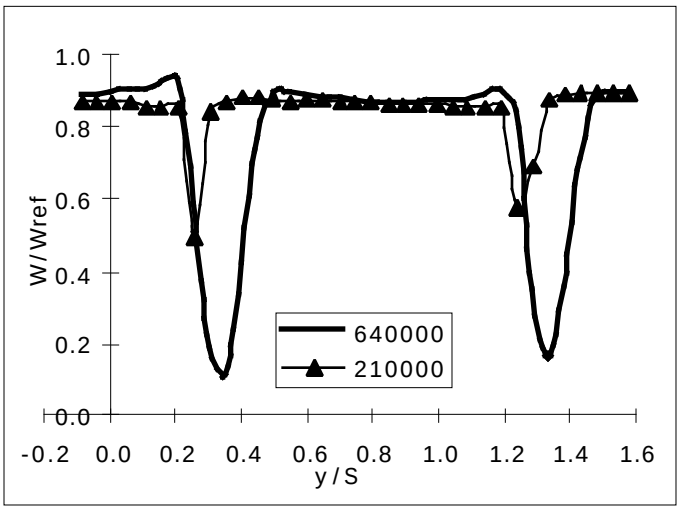

Fig. 9 Wake profiles at 38° inlet flow angle for the highest and lowest Reynolds number flows.

First, periodicity is evident in both profiles; and second the significantly larger wake width and deficit for the high Reynolds number case is evident. At this station the minimum velocity was only 10% of the core flow. At preceding stations, reverse flow was measured, which indicated that the trailing edge had separated. The individual velocity components for the wake distributions for all three Reynolds numbers were presented in Schnorenberg (1996).

The exit flow angle distributions for the high and low Reynolds number cases were also significantly different as shown in Fig. 10. At the high Reynolds number the mass-averaged exit flow angle was 9.25°, and this value decreased with decreasing Reynolds number to 4.56°

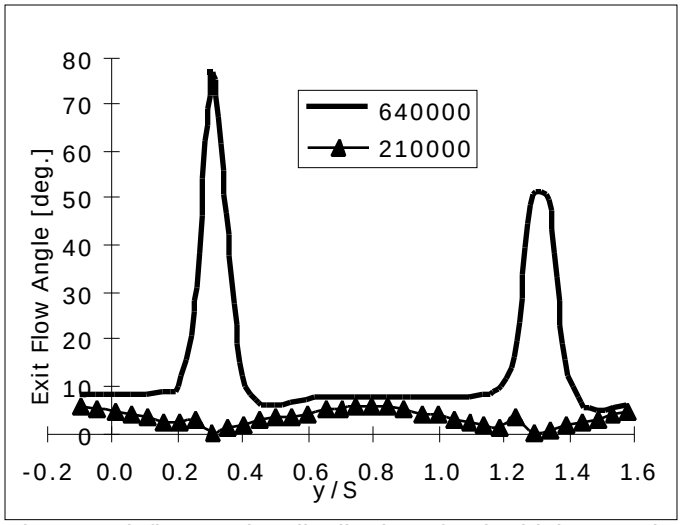

Fig. 10 Exit flow angles distributions for the highest and lowest Reynolds number flows.

and 3.74° respectively for Reynolds numbers of 380,000 and 210,000. At the 640,000 Reynolds number the peak flow angle in the wake was in excess of 50°, and the flow angle distribution between the blades was relatively uniform, whereas for 210,000 Reynolds number the flow angle in the core flow showed a maximum half way between the blades. This profile was similar to the design exit flow angle distribution measured at the high Reynolds number by Hansen (1995).

The exit turbulence distributions are shown in Fig. 11, where the profile for the separated boundary layer showed the double peaked distribution. Each peak corresponded to the maximum velocity gradient shown in Fig. 9. The resolution of the measurements for the low Reynolds number test case were not sufficient to resolve the aforementioned double peak distribution.

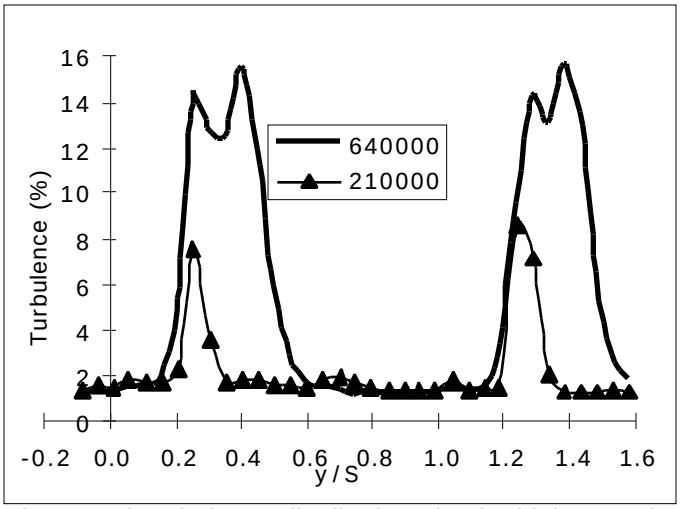

Fig. 11 Exit turbulence distributions for the highest and lowest Reynolds number flows.

Good periodicity was evident in the turbulence profiles when compared to the exit flow angle distributions in Fig. 10. The freestream turbulence was measured to be approximately 1.4% for all three Reynolds numbers, although the inlet turbulence was inversely proportional to Reynolds number as shown in Table 3.

Suction Surface Boundary Layers

Total velocity and turbulence distributions are presented in Figs. 12 and 13 at stations 5, 6, 7, 8 and 9 for the high and intermediate Reynolds numbers. At the high Reynolds number reverse flow was measured at stations 8 and 9 with corresponding increased turbulence levels. As noted by the flow visualization Fig. 6, the flow over the suction surface was three dimensional and so these two-component measurements need to be interpreted accordingly.

No reverse flow was measured at the intermediate Reynolds number (Fig. 13). This could be due to the spanwise variation of axial transition location on the suction surface. When transition had occurred boundary layer separation was suppressed as shown in Fig. 7. The LDV measurements were taken over a region where transition had occurred as is evident by the increase of turbulence in the boundary layer at stations 5, 6 and 7. The blade surface pressure measurements, which showed a separation bubble plateau for the intermediate Reynolds number, were taken on blade no. 6 (Fig. 1) and all the LDV measurements were performed between blades 3 and 4. Another explanation for the reason for differing LDV and pressure measurements, could be due to the spanwise variation of the separation bubble at the transitional Reynolds number of 380,000.

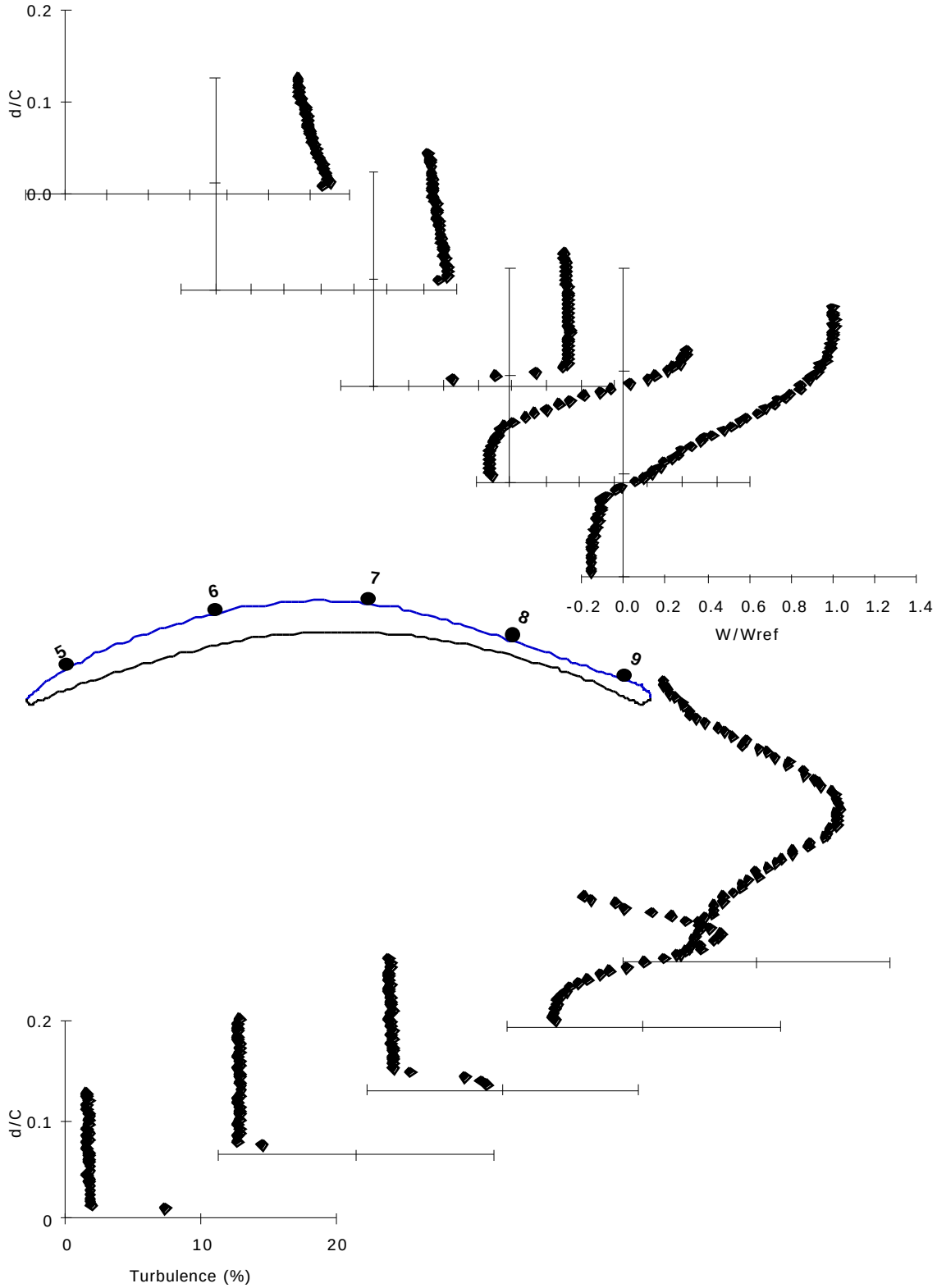

Fig. 12 Suction-surface boundary-layer profiles at 640,000 Reynolds no.

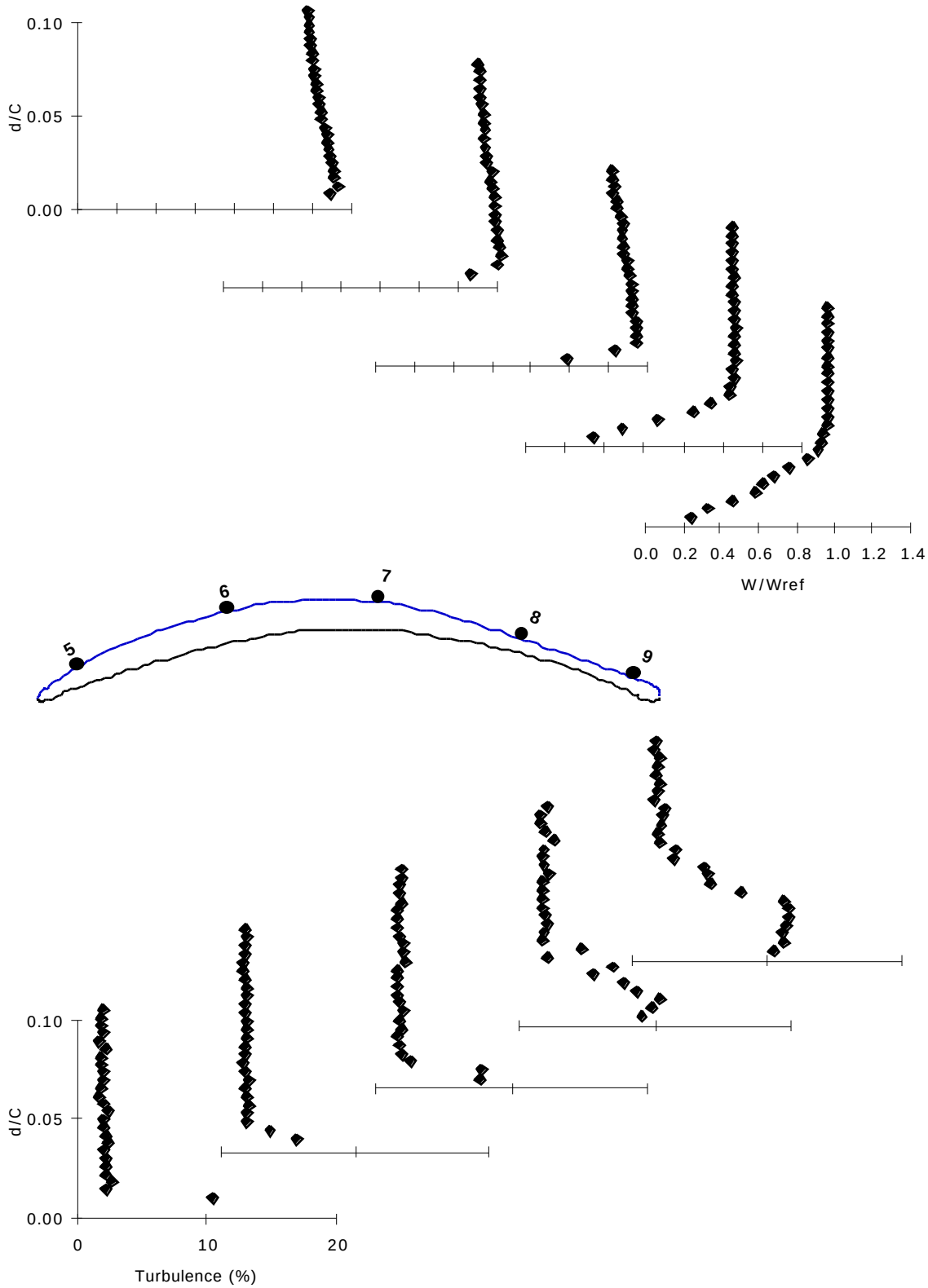

Fig. 13 Suction-surface boundary-layer profiles at 380,000 Reynolds no.

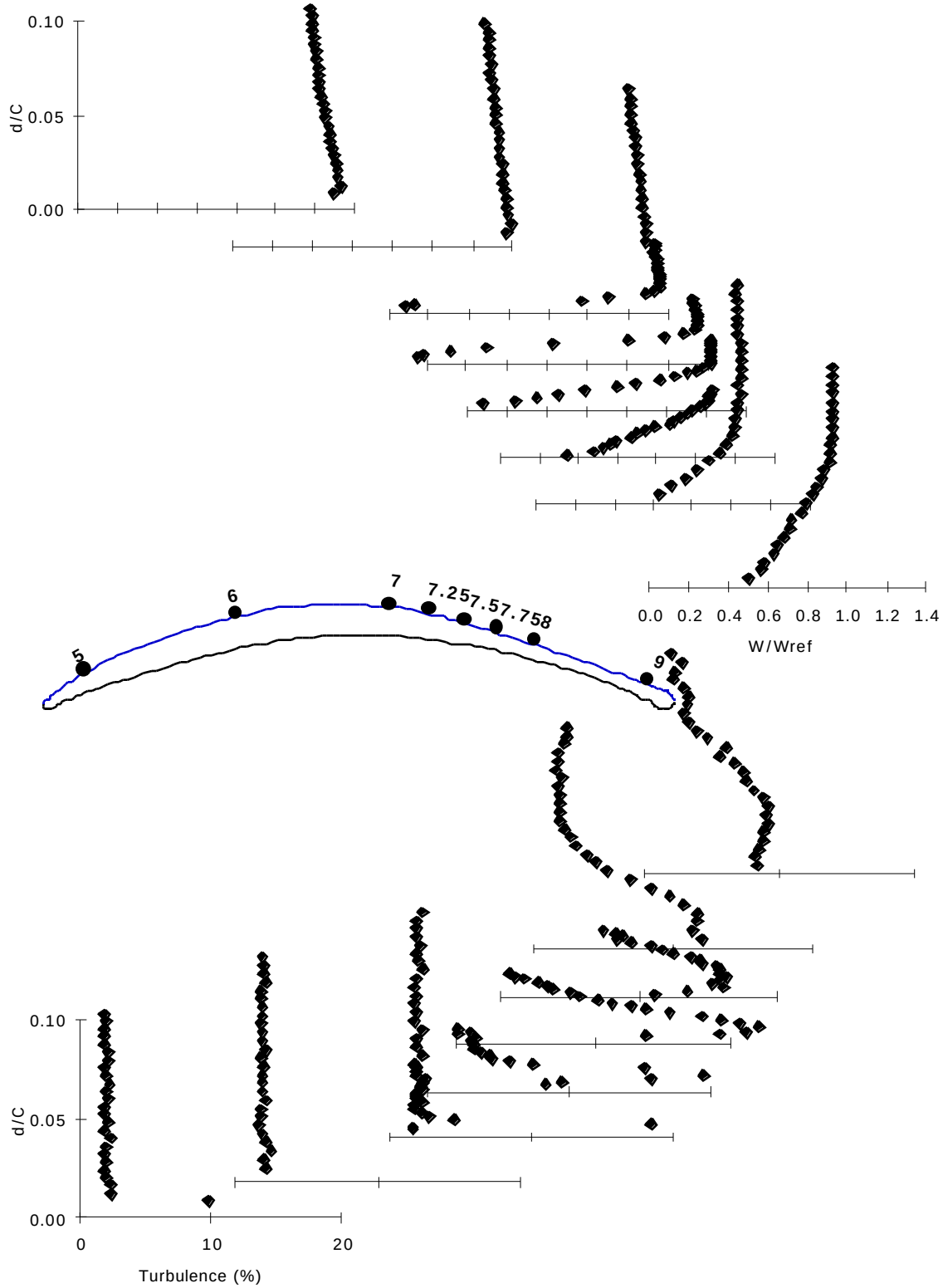

Fig 14. Suction-surface boundary-layer profiles at 210,000 Reynolds number.

At the lowest Reynolds number (Fig. 14) reverse flow was measured at station 7.25 (25% axial distance between stations 7 and 8) at the first two points away from the blade surface. As can be seen from the upstream profiles, the state of the boundary layers was laminar because of the reduced turbulence levels.

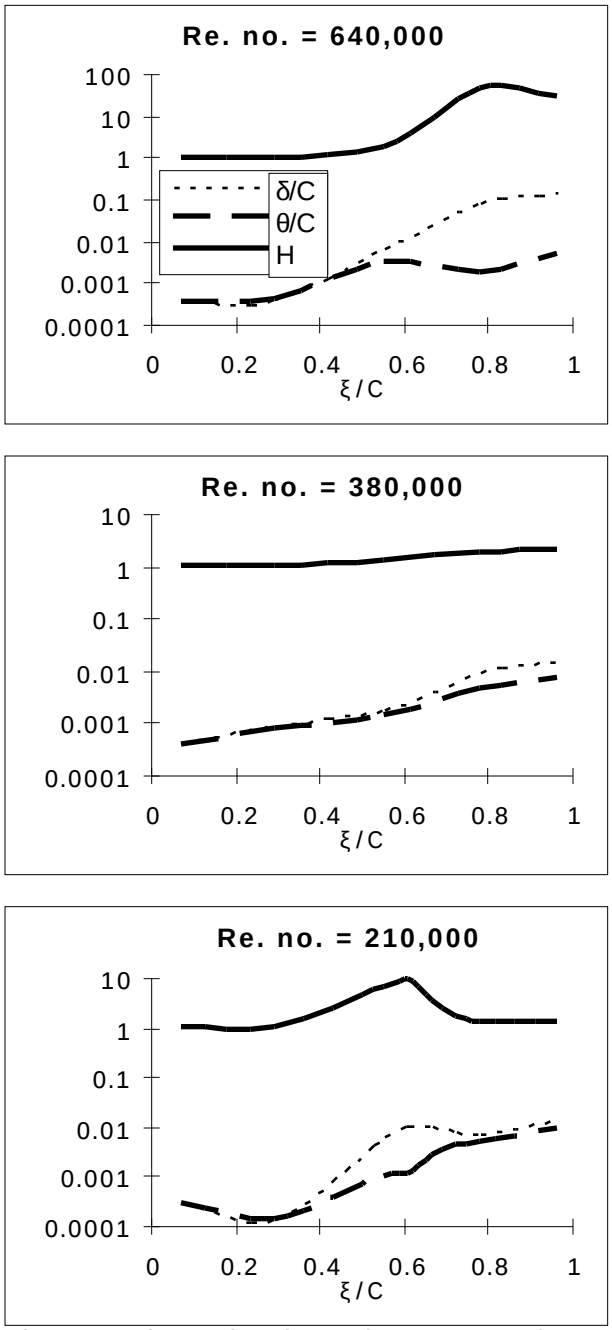

Fig. 15 Suction surface integral parameters of displacement thickness, momentum thickness and shape factor for the three Reynolds numbers.

By station 7.75 the profile exhibited the character of a reattached turbulent boundary layer, with increased growth rate and increased turbulence levels. At the last two stations (8 and 9) the turbulence profile exhibited a double peaked distribution. The outer peak being due to the free shear layer over the bubble and inner peak being due to the reformation of the attached boundary layer. When comparing the relative size of the boundary layers between the high Reynolds number case and the low Reynolds number case, it can be seen that the separated boundary profile (Fig. 12, station 9) is larger than the attached profile (Fig. 14). In Fig. 15 the displacement thickness for the high Reynolds number case is an order of magnitude larger at the trailing edge than the low Reynolds number test case. For both the separated flow regions, at the high and low Reynolds number, there is a localized increase in displacement thickness and shape factor with a leveling off of the momentum thickness. At the intermediate Reynolds number the integral parameters increase continually along the suction surface.

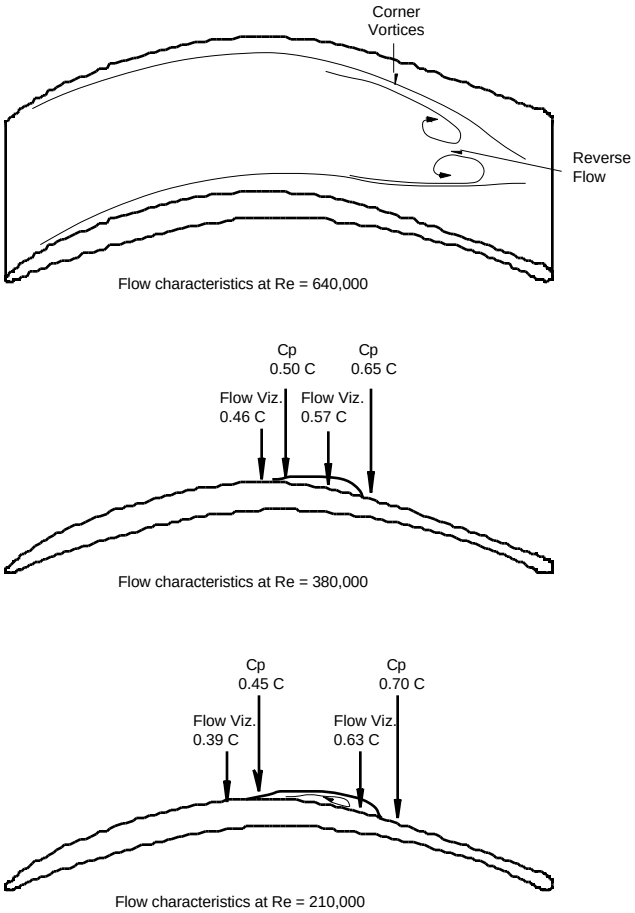

Fig. 16 Flow structure variation with Reynolds number.

Summary

In summary, Fig. 16 shows the approximate flow structure for the three Reynolds numbers. The experimentally determined separation and reattachment locations for the low and intermediate Reynolds number cases are indicated. The region of flow reversal determined from flow visualization and LDV measured separation for the high Reynolds number case are also shown with the vortex structure on the blade surface. The three measurement techniques (flow visualization, surface pressure measurements and LDV) all agree reasonably well, giving confidence in the proposed flow structure. Although the coarseness of the location of the LDV surveys precludes determining the separation point exactly, reverse flow measurements were obtained at the location between separation and reattachment for the low Reynolds number test case.

CONCLUSIONS

Detailed laser-Doppler anemometry measurements of the flow over the suction surface of a set of second-generation controlled-diffusion compressor stator blades showed that as the Reynolds number was decreased from the design value of approximately 640,000 to 210,000 a laminar separation bubble, which reattached turbulent, formed at mid chord. The flow also became more two dimensional as the effect of the corner vortices were diminished as the Reynolds number was decreased. At the high Reynolds number the trailing edge experienced turbulent flow reversal as a result of the interaction of the corner vortices. At the intermediate Reynolds number of 380,000 separation occurred on the suction surface when the approaching boundary layer remained laminar, however; when the boundary had undergone transition to turbulent flow then separation was suppressed which gave rise to a spanwise variation of the separation bubble.

Additional pressure measurements and surface flow visualization confirmed the results obtained quantitatively with the LDV. These data should form a challenging test case for viscous flow calculations, particularly for the calibration of turbulence models and their ability to predict the effect of Reynolds number on the state of a boundary layer.

ACKNOWLEDGEMENTS

This work was sponsored by the Naval Air Warfare Center (Patuxent River), as part of a Fan and Compressor Stall Project. Mr. Stoney McAdams was technical monitor for the project, and his support is greatly appreciated.

REFERENCES

Elazar, Y.,1988, "A Mapping of the Viscous Flow Behavior in a Controlled-Diffusion Compressor Cascade Using Laser Doppler Velocimetry and Preliminary Evaluation of Codes for the Prediction of Stall," Ph. D. Dissertation, Naval Postgraduate School.

Evans, B. J., 1971, "Effects of Free-Stream Turbulence on Blade Performance in a Compressor Cascade," Cambridge Univ., Engineering Dept., Turbo/TR 26.

Gelder, T. F., Schmidt, J. F., Suder, K. L. and Hathaway M. D., 1989, "Design and Performance of Controlled-Diffusion Stator Compared with Original Double-Circular-Arc Stator," NASA TP 2852.

Grove, D. V., 1971, "Experimental and Numerical Investigation of Second-Generation, Controlled-Diffusion, Compressor Blades in Cascade," Master of Science in Aeronautical Engineering, Naval Postgraduate School.

Hansen, D. J., 1995, "Investigation of Second-Generation Controlled-Diffusion Compressor Blades in Cascade," Master of Science in Aeronautical Engineering, Naval Postgraduate School.

Hobson, G. V., and Shreeve, R. P., 1993, "Inlet Turbulence Distortion and Viscous Flow Development in a Controlled-Diffusion Compressor Cascade at Very High Incidence," AIAA *Journal of Propulsion and Power* , Vol. 9, No. 3, pp 397-404.

Horlock, J. H., Shaw, R., Pollard, D., and Lewkowicz, A., 1964, "Reynolds Number Effects in Cascades and Axial Flow Compressors," ASME Trans., Series A, *Journal of Engineering for Power*.

Johnsen, I. A., and Bullock, R. O., 1965, (Editors) "Aerodynamic Design of Axial-Flow Compressors," NASA SP-36.

Roberts, W. B., 1975, "The Effect of Reynolds Number and Laminar Separation on Axial Cascade Performance," *Journal of Engineering for Power*, Vol 97, Series A, No. 2, pp 261-274.

Rhoden, H. G., 1956, "Effect of Reynolds Number on the Flow of Air through a Cascade of Compressor Blades," ARC, R & M 2919.

Sanger, N. L., 1982, "The Use of Optimization Techniques to Design Controlled-Diffusion Compressor Blading," NASA T. M. 82763, also ASME 82-GT-149.

Schlichting, H., and Das, A., 1970, "On the Influence of Turbulence Level on the Aerodynamic Losses of Axial Turbomachines," from *Flow Research on Blading,* ed. L. S. Dzung, Elsevier Publ. Co.

Schnorenberg, D. G., 1996, "Investigation of the Effect of Reynolds Number on Laminar Separation Bubbles on Controlled-Diffusion Compressor Blades in Cascade," Master of Science in Aeronautical Engineering, Naval Postgraduate School.

Appendix:- Blade coordinates in mm (Fig. 2)

ξ	η	ξ	η	ξ	η	ξ	η	ξ	η	ξ	η
-0.02	0.74	42.22	20.63	114.06	8.20	126.77	0.60	98.46	10.69	27.66	9.83
-0.01	0.82	43.53	20.90	114.88	7.89	126.69	0.53	97.21	11.03	26.44	9.46
-0.01	0.90	44.84	21.16	115.69	7.58	126.60	0.45	95.97	11.37	25.21	9.09
0.01	0.97	46.14	21.40	116.51	7.27	126.48	0.38	94.72	11.69	24.01	8.71
0.03	1.05	47.48	21.62	117.32	6.97	126.38	0.32	93.48	12.00	22.80	8.34
0.06	1.13	48.81	21.82	118.14	6.66	126.30	0.28	92.23	12.30	21.59	7.95
0.09	1.20	50.14	22.00	118.95	6.36	126.22	0.25	90.97	12.58	20.38	7.56
0.13	1.28	51.48	22.16	119.57	6.13	126.15	0.22	89.72	12.86	19.18	7.16
0.17	1.35	52.81	22.29	120.18	5.90	125.99	0.17	88.46	13.11	17.97	6.76
0.22	1.43	54.14	22.40	120.80	5.68	125.77	0.12	87.20	13.36	16.97	6.42
0.28	1.51	55.49	22.49	121.41	5.45	125.31	0.08	85.95	13.60	15.98	6.08
0.35	1.58	56.84	22.55	122.03	5.22	125.08	0.09	84.69	13.83	14.98	5.73
0.42	1.66	58.18	22.59	122.64	4.98	124.93	0.11	83.44	14.05	13.98	5.37
0.75	1.98	59.53	22.60	123.04	4.82	124.70	0.14	82.18	14.26	12.99	5.02
1.07	2.29	60.88	22.59	123.45	4.65	124.55	0.18	80.92	14.46	11.99	4.65
1.40	2.60	62.22	22.56	123.85	4.49	124.39	0.22	79.66	14.65	11.21	4.36
1.72	2.89	63.57	22.50	124.25	4.32	124.24	0.27	78.41	14.83	10.42	4.07
2.04	3.19	64.91	22.42	124.65	4.14	124.09	0.32	77.15	15.00	9.64	3.77
2.37	3.47	66.25	22.31	125.05	3.96	124.01	0.35	75.90	15.15	8.86	3.47
2.90	3.91	67.59	22.18	125.23	3.88	123.94	0.38	74.64	15.28	8.07	3.16
3.42	4.34	68.93	22.03	125.38	3.80	123.86	0.41	73.39	15.41	7.29	2.83
3.95	4.76	70.27	21.85	125.52	3.73	123.78	0.45	72.14	15.51	6.71	2.59
4.47	5.16	71.58	21.65	125.65	3.65	123.71	0.48	70.88	15.60	6.12	2.33
5.00	5.55	72.88	21.42	125.77	3.58	123.63	0.52	69.63	15.67	5.54	2.07
5.53	5.93	74.19	21.17	125.88	3.50	123.56	0.56	68.38	15.73	4.96	1.81
6.28	6.46	75.50	20.90	125.98	3.42	123.48	0.60	67.13	15.77	4.37	1.54
7.03	6.97	76.81	20.61	126.08	3.35	123.39	0.66	65.88	15.80	3.79	1.27
7.78	7.46	78.12	20.29	126.17	3.27	123.03	0.90	64.64	15.81	3.41	1.09
8.53	7.93	79.39	19.97	126.26	3.20	122.66	1.13	63.39	15.81	3.02	0.91
9.28	8.39	80.67	19.64	126.34	3.12	122.30	1.35	62.14	15.79	2.64	0.72
10.03	8.83	81.94	19.29	126.41	3.04	121.94	1.57	60.90	15.77	2.26	0.54
11.01	9.39	83.21	18.93	126.48	2.97	121.58	1.78	59.66	15.73	1.87	0.35
11.99	9.92	84.49	18.56	126.55	2.89	121.21	1.99	58.42	15.69	1.49	0.17
12.97	10.42	85.76	18.18	126.61	2.81	120.64	2.30	57.18	15.63	1.42	0.13
13.95	10.91	87.01	17.80	126.67	2.74	120.07	2.59	55.94	15.55	1.34	0.10
14.93	11.39	88.26	17.41	126.72	2.66	119.51	2.88	54.70	15.46	1.27	0.07
15.91	11.84	89.50	17.01	126.77	2.59	118.94	3.16	53.47	15.35	1.19	0.05
17.12	12.40	90.75	16.61	126.82	2.51	118.37	3.43	52.24	15.23	1.12	0.03
18.34	12.93	92.00	16.19	126.86	2.43	117.80	3.70	51.00	15.09	1.04	0.01
19.55	13.45	93.25	15.77	126.90	2.36	117.02	4.07	49.77	14.93	0.96	0.00
20.77	13.96	94.48	15.34	126.94	2.28	116.24	4.43	48.53	14.75	0.89	0.00
21.98	14.44	95.70	14.90	126.97	2.20	115.45	4.78	47.30	14.56	0.81	-0.01
23.20	14.92	96.93	14.46	127.00	2.13	114.67	5.12	46.07	14.35	0.73	0.00
24.44	15.38	98.16	14.01	127.03	2.05	113.89	5.46	44.83	14.12	0.66	0.00
25.68	15.83	99.38	13.56	127.05	1.98	113.11	5.79	43.60	13.88	0.58	0.02
26.93	16.27	100.61	13.11	127.07	1.90	112.11	6.20	42.37	13.62	0.51	0.04
28.17	16.70	101.84	12.67	127.09	1.82	111.11	6.60	41.14	13.36	0.43	0.07
29.41	17.11	103.06	12.23	127.11	1.67	110.10	6.99	39.90	13.08	0.35	0.10
30.66	17.51	104.28	11.79	127.12	1.48	109.10	7.36	38.68	12.79	0.29	0.13
31.93	17.91	105.51	11.35	127.11	1.29	108.10	7.72	37.45	12.50	0.20	0.21
33.21	18.29	106.73	10.91	127.08	1.14	107.09	8.06	36.23	12.19	0.13	0.29
34.48	18.67	107.96	10.47	127.05	1.06	105.86	8.48	35.00	11.88	0.08	0.36
35.76	19.03	108.97	10.10	127.00	0.99	104.63	8.87	33.78	11.56	0.04	0.44
37.03	19.37	109.99	9.72	126.99	0.91	103.40	9.25	32.55	11.23	0.01	0.52
38.31	19.70	111.01	9.35	126.95	0.83	102.17	9.62	31.33	10.89	-0.01	0.59
39.61	20.03	112.03	8.97	126.90	0.76	100.94	9.99	30.11	10.54	-0.01	0.67
40.92	20.34	113.04	8.59	126.84	0.68	99.70	10.34	28.88	10.19	-0.02	0.74